Characterization and Prediction of Femtosecond Laser Induced Tracks in Silver-Containing Zinc Phosphate Glass

Luttfi A. Al-Haddad[1], Alaa Abdulhady Jaber[2], Mohamed K. Dhahir[3], Hagir Y. Nagim[3] and Zahraa Ihsan Algburi[2]

[1]Training and Workshops Center, University of Technology- Iraq, Baghdad, Iraq
[2]Mechanical Engineering Department, University of Technology- Iraq, Baghdad, Iraq
[3]Laser Institute for Postgraduate Studies, University of Baghdad, Baghdad, Iraq

Abstract

Femtosecond laser writing is capable of producing highly localized, volumetric changes within materials, which provide the foundations for using the material to create 3D photonic structures. The present work deals with the formation of femtosecond laser-induced tracks in silver containing zinc phosphate glass, for the study of the effect of laser parameters, like the pulse repetition rate, by varying the parameters from 10, 100 to 500 kHz and pulse energy from 60 to 120 nJ. The changes in microstructure and optical properties are recorded through optical microscopy in both brightfield and fluorescence modes, with a specific interest in the dimensions of the laser-written tracks. This study was conducted using an Artificial Neural Networks (ANN) to predict the width and height of the tracks based on the varying laser exposure parameters. The analysis includes a comprehensive assessment of prediction accuracy through Mean Squared Error (MSE), Root Mean Squared Error (RMSE), Mean Absolute Error (MAE), Mean Absolute Percentage Error (MAPE), Coefficient of Variation of the Root Mean Squared Error (CVRMSE), and determination coefficient (R^2) with expected values denoted as 0.232%, 0.482%, 0.312%, 0.066%, 10.241%, and 0.909 respectively. These metrics do show the effectiveness and reliability of the ANN model in capturing the complex dynamics of the laser material processing phenomenon. In fact, these resourceful predictions are a mile toward the real optimization of laser processing techniques in material science—a quantitative tool for the prediction of material responses under varied laser settings.

Keywords

Phosphate glass, Femtosecond laser tracks, Artificial intelligence, Artificial neural network

1. Introduction and Literature Review

The recent breakthroughs in femtosecond laser technology have inaugurated a novel paradigm within material science, facilitating unparalleled control over the manipulation of material properties on the micro and nanoscale [1, 2, 3]. Similarly, the integration of technologies has been demonstrated in other fields, such as in telecommunications for enhancing real-time events [4, 5, 6, 7, 8], and in public health through IoT and computer vision for ensuring health safety. Femtosecond lasers, distinguished by their exceptionally brief pulse durations, enable localized modifications within materials, circumventing the substantial thermal damage typically observed with longer pulse durations. It is particularly important for Non-Terrestrial Networks (NTNs) [9]. Significant advancement represents a paramount contribution to the field of photonics and advanced material engineering, where the structural integrity and performance characteristics of materials must be rigorously maintained throughout processing [10]. The realization of nanoscale structuring with exceptional resolution highlights the paradigm-shifting potential of this technique [11].

Zinc phosphate glasses containing silver, lauded for their exceptional potential in photonic applications and devices, have garnered significant interest as promising candidates for femtosecond laser processing. The incorporation of silver not only serves to augment the glass's optical properties, such as its refractive index and nonlinear optical response, but also unlocks avenues for groundbreaking advancements in high-density optical data storage and waveguide fabrication [12]. The meticulous control over material properties achievable with femtosecond lasers is instrumental in propelling the application of these materials in next-generation optical technologies, and emphasizes the crucial need for a thorough understanding of laser-material interactions [10, 13]. Contemporaneous investigations into femtosecond laser processing of glasses have unveiled promising advancements in the microscale manipulation of optical properties. Shakhgildyan et al. have demonstrably shown

SYSYEM 2024: 10th Scholar's Yearly Symposium of Technology, Engineering and Mathematics, Rome, December 2-5, 2024
Luttfi.a.alhaddad@uotechnology.edu.iq (L. A. Al-Haddad); Alaa.a.jaber@uotechnology.edu.iq (A. A. Jaber); Mohammed@ilps.uobaghdad.edu.iq (M. K. Dhahir); Hager.y@ilps.uobaghdad.edu.iq (H. Y. Nagim)
0000-0001-7832-1048 (L. A. Al-Haddad); 0000-0001-5709-195X (A. A. Jaber); 0009-0005-5916-6632 (M. K. Dhahir); 0009-0000-5683-765X (H. Y. Nagim); 0009-0000-7572-057X (Z. I. Algburi)

that femtosecond direct laser writing (DLW) can induce luminescence, absorption, and generate birefringence within micron-sized regions of silver-doped zinc phosphate glasses, obviating the need for subsequent thermal treatment [14]. Subsequent in-depth investigations by Guérineau et al. have significantly enhanced the comprehension of these phenomena. Their work has introduced the concept of Type AC and AN modifications, encompassing both silver clusters and nanoparticles, thereby refining the existing classification system for microstructural modifications within glasses [15]. This meticulous control over material properties at the micron scale represents a critical facet in the development of novel photonic devices. Alassani et al. have demonstrably achieved success in inscribing three-dimensional luminescent patterns that achieve co-localization of silver clusters and rare-earth ions. This achievement underscores the potential for groundbreaking advancements in novel optical data storage and sensor applications [16, 17]. Concurrently, the research conducted by Lv et al. exemplifies the fabrication of cladding waveguides in proximity to the glass surface. This strategic positioning optimizes the interaction of light with the modified regions, thereby facilitating enhanced photonic integration [18, 19].

Beyond the conventional structuring of waveguides, the femtosecond laser has been leveraged to create intricate photonic structures within glass. Tsimvrakidis et al. have delved into the reversible inscription of waveguides in silver phosphate glasses, thereby paving the way for the realization of dynamically reconfigurable photonic circuits [20]. In a similar vein, Guérineau et al. have documented their success in employing direct laser writing (DLW) to fabricate subwavelength periodic structures within mid-infrared glasses. This achievement signifies a novel level of control over the manipulation of optical properties facilitated by DLW [21]. Desmoulin et al. further elucidated this capability of tailoring the glass's microstructure at sub-micron scales. Their work demonstrably showcased selective etching and post-laser writing surface topography engineering, thereby highlighting the potential for intricate surface structuring in photonic applications [22]. At a foundational level, the investigations by Bukharin et al. have significantly augmented the comprehension of the heat accumulation regime governing femtosecond laser writing. Their work has meticulously elucidated how adjustments in laser parameters can exert fine-grained control over modifications in refractive index and waveguide properties [23]. Collectively, these advancements significantly enrich the repertoire of tools available to engineers specializing in the design of cutting-edge optical materials and devices. This enrichment is driven by the ability to harness the unique properties of silver-containing glasses, which are further accentuated through femtosecond laser interactions. Table 1 subsequently presents a succinct compilation of these pivotal studies, offering a concise overview of the investigated materials and the reported discoveries.

Following a critical examination of the key studies summarized in Table 1 regarding femtosecond laser writing in photonic glasses, it becomes apparent that significant strides have been made in comprehending and employing femtosecond laser technologies for micro- and nanoscale structuring within diverse glass compositions. However, certain areas warrant further exploration. The majority of existing research has primarily concentrated on manipulating physical properties such as refractive index alterations and the fabrication of luminescent patterns. Conversely, less emphasis has been placed on the development of predictive models for these changes and a comprehensive analysis of how varying laser parameters influence the physical and optical properties of silver-containing zinc phosphate glasses. Additionally, while some studies have leveraged Artificial Intelligence (AI) for pattern inscription and modifications, the application of Artificial Neural Networks (ANNs) to predict outcomes based on laser parameters remains relatively undocumented in the context of optimizing femtosecond laser processes.

This lacuna underscores the necessity for a systematic approach to prognosticate and optimize the properties of materials processed with femtosecond lasers. This is precisely where the current research intervenes. The study meticulously documents the microstructural modifications induced by varying laser parameters and presents a pioneering application of ANNs to achieve accurate predictions of laser-written track dimensions. The following highlights the paper's principal contributions:

· Leveraging an Artificial Neural Network (ANN) to achieve accurate predictions of track dimensions through comprehensive consideration of diverse laser parameters.

· In-depth investigation of the influence exerted by pulse repetition rates and pulse energy on track formation.

· Concurrent implementation of both brightfield and fluorescence microscopy to evaluate changes, providing a multifaceted approach to optical characterization.

· Employing a battery of error assessment metrics to rigorously validate the predictive accuracy of the ANN model.

2. Experimental Methodology: Design, Materials and Methods

To investigate the formation of laser-induced tracks in silver-containing zinc phosphate glass, a detailed experimental setup was employed using a Yb:KGW femtosecond laser system named Pharos SP, Light Conversion Ltd [26]. with a regenerative amplifier. The laser, operating at a wavelength of 1030 nm, was precisely controlled to

Table 1
Summary of key studies on femtosecond laser writing in photonic glasses

Ref.	Material Studied	Key Findings	Experimental	AI/Expert System
[14]	Silver-doped zinc phosphate glasses	Joint formation of fluorescent silver clusters and plasmonic silver nanoparticles without heat treatment.	Yes	No
[15]	Phosphate glass	Classification of microstructure modifications in glass (type AC and AN) depending on laser parameters.	Yes	No
[16]	Yb3+ and silver-containing phosphate glass	Demonstration of DLW to inscribe 3D luminescent patterns utilizing co-localization of silver clusters and Yb3+ ions.	Yes	Yes
[18]	Yb-doped phosphate glass	Fabrication of cladding waveguides with controlled light propagation using a femtosecond laser.	Yes	No
[20]	Silver metaphosphate glass	Reversible inscription of waveguides allowing dynamic photonic device configuration.	Yes	Yes
[21]	Mid-Infrared Gallo-Germanate Glass	Embedding subwavelength periodic structures inside optical materials.	Yes	Yes
[22]	Silver-containing phosphate glass	Permanent formation of fluorescent structures and surface topology engineering through laser structuring.	Yes	No
[23]	Fused silica and Nd	Studied heat accumulation regime in femtosecond laser writing affecting refractive index.	Yes	No
[24]	Silver-containing sodium-gallium phosphate glasses	Influence of glass network structure on laser-writing properties and photosensitivity.	Yes	No
[25]	Silver-containing sodo-gallo-phosphate glasses	Investigation of silver species generation under X-ray and femtosecond laser exposure.	Yes	No

emit pulses with a duration of 180 fs at repetition rates of 10, 100, and 500 kHz. The energy of these pulses was varied from 60 to 120 nJ using a motorized polarization attenuator, while a motorized half-wave plate was utilized to align the linear polarization of the laser beam parallel to the scanning direction.

The focused laser beam was directed into the volume of a glass plate, measuring $0.4 \times 1.5 \times 2.5cm$, positioned on an air-bearing stage (Aerotech ABL1000). This setup, synchronized with the laser system via SCA Professor software, facilitated precise 3D positioning of the glass sample at a constant scanning speed of 1 mm/s and maintained a fixed focus depth of 150 μm. To avoid overlapping, a spacing of 200 μm between the tracks was maintained throughout the experiment.

The glass used in these experiments was silver-containing zinc phosphate glass with a composition of 8Ag20, 53ZnO, 39P2O5 (mol%) [27]. This glass was synthesized using a melt-quenching technique from high-purity precursors (AgNO3, ZnO, H3PO4) [27]. The mixture was heated to 1200 °C in a corundum crucible covered with a fused silica cap and held for two hours before being rapidly quenched in a preheated metal mold and annealed at 325 °C for four hours to reduce mechanical stresses. The resulting glass block was processed into optically polished plates suitable for laser treatment experiments.

To characterize the microstructure and optical properties of the laser-written tracks, optical microscopy was conducted in both brightfield and fluorescence modes using an Olympus BX51 microscope equipped with an Olympus DP73 CCD camera. Brightfield images were taken to visualize the tracks (Figure 1a), and fluorescence images were captured under excitation between 400–410 nm, with emission registered in the 455–800 nm range (Figure 1b). The exposure times for these images were 200 ms for top-view configurations and 100 ms for cross-section views. Image analysis was performed using ImageJ software to quantify the dimensions and optical characteristics of laser modifications [28].

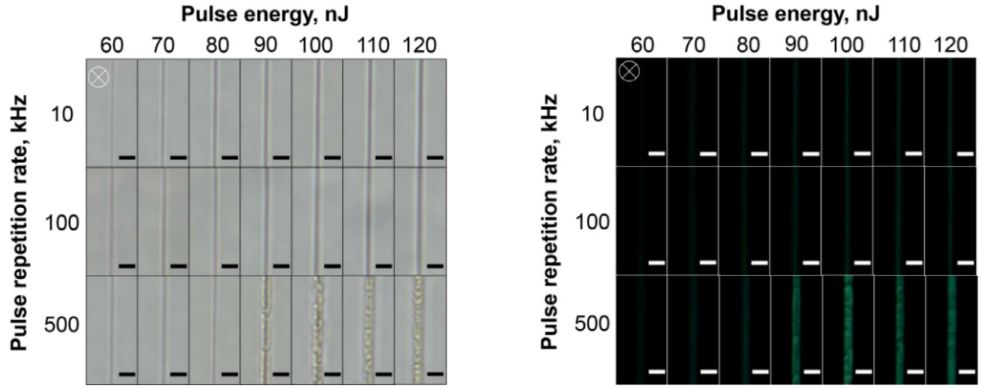

(a) (b)

Figure 1: Composite microscopic analysis of laser-induced tracks in silver-containing zinc phosphate glass: (a) Brightfield microscopy; (b) Fluorescence microscopy [19]Composite microscopic analysis of laser-induced tracks in silver-containing zinc phosphate glass: (a) Brightfield microscopy; (b) Fluorescence microscopy [26]

3. AI Expert System

3.1. Artificial Neural Network

The integration of AI technologies has revolutionized numerous fields, ranging from autonomous driving to energy production and dispatch, from robotics to personalized medicine [29, 30, 31, 32, 33, 34, 35, 36, 37]. Among these technologies, Artificial Neural Networks (ANNs) have emerged as a powerful tool for modeling complex and nonlinear relationships that defy traditional analytical approaches [38, 39, 40, 41, 42, 43, 44, 45, 46, 47]. ANNs are widely used across various applications to predict outcomes, optimize processes, and understand intricate patterns in data [48, 49, 50]. For this study, an ANN was employed to predict the dimensions of femtosecond laser-induced tracks in silver-containing zinc phosphate glass. The ANN architecture was designed to approximate the functional relationship between the input laser parameters and the resulting track dimensions. The model's structure is represented by the following equations 1 to 3:

$$y = f\left(\sum_{i=1}^{n}(w_i x_i + b)\right) \tag{1}$$

$$f = \tanh(x) = \frac{\sinh(x)}{\cosh(x)} = \frac{e^x - e^{-x}}{e^x + e^{-x}} \tag{2}$$

$$w_{\text{new}} = w_{\text{old}} - \eta \nabla Q(w_{\text{old}}, x_i, y_i)] \tag{3}$$

Where y is the output, w_i represents the weight, x_i are representing the input values, and b is for the bias. The activation function is represented by f, and η is the learning rate. The configuration of the neural network, as detailed in Table 2, includes two hidden layers with four neurons in the first layer and two in the second, utilizing Stochastic Gradient Descent (SGD) as the solver over 250 iterations. This setup was optimized to capture the nuances of how varying laser parameters influence the physical properties of the tracks formed.

Table 2
Parameters for the neural network

Parameter	Value
Number of hidden layers	2
Number of neurons in first hidden layer	2
Number of neurons in second hidden layer	4
Solver	SGD
Number of iterations	250

3.2. Model Assessment Metrics

Following are several statistics important in the predictive model's appraisal for accuracy and reliability:

· MSE: The Mean Squared Error is the average of squares of the errors as equation 4 states. Though differences of predicted and true values provide some insight into the magnitude of the errors, this measure can be very sensitive to outliers.

· RMSE: Root Mean Squared Error is the square root of MSE computer using equation 5 [51]. It yields a measure of the same errors in the same units as the response variable; hence, it is more interpretable.

· MAE: Mean Absolute Error gives the average absolute difference in predicted and actual values as indication in the formula 6, and it gives a very direct indication of the accuracy of the prediction but does not show in what direction the error is.

· MAPE: Mean Absolute Percentage Error shows accuracy in percentage as enlisted in equation 7. It gives a very clear perspective of the size of errors relative to true values which is very helpful when comparing error in different datasets of different scales.

· CVRMSE: Coefficient of Variation of the Root Mean Squared Error is a normalized measure of RMSE as equation 8 indicates, making it an important and very useful metric for comparing relative prediction error in different datasets or models [52].

· R^2: The Coefficient of Determination explains the proportion of variance in the dependent variable predicted from the independent variables. It serves as an indicator of the goodness of fit of the model; a higher R^2 says the model is more capable of capturing variability in data, it can be calculated using equation 9 [53].

$$\text{MSE} = \frac{1}{m}\sum_{i=1}^{m}(x_i - y_i)^2 \tag{4}$$

$$\text{RMSE} = \sqrt{\frac{1}{m}\sum_{i=1}^{m}(x_i - y_i)^2} \times 100 \tag{5}$$

$$\text{MAE} = \frac{1}{m}\sum_{i=1}^{m}|x_i - y_i| \tag{6}$$

$$\text{MAPE} = \frac{\text{RMSE}}{\bar{x}} \times 100 \tag{7}$$

$$\text{CVRMSE} = \frac{\text{RMSE}}{\bar{x}} \times 100 \tag{8}$$

$$R^2 = \frac{\left(\sum_{i=1}^{m}(x_i - \bar{x})(y_i - \bar{y})\right)^2}{\sum_{i=1}^{m}(x_i - \bar{x})^2 \times \sum_{i=1}^{m}(y_i - \bar{y})^2} \tag{9}$$

These metrics are essential methods to be included in building evaluation frameworks to test predictive models and refine them to ensure their practical application.

4. Results and Analysis

4.1. Data Visualization and Experimental Results

To explore the influence of pulse energy on height, the experiment systematically varied the pulse energy from 60 nanojoules (nJ) to 120 nJ. Subsequently, the height parameter ("heightg") was measured in triplicate at each pulse repetition rate: 10 kHz, 100 kHz, and 500 kHz. To assess measurement reliability, the mean and percentage error were calculated for each set of three height measurements. The experiment was then replicated for all three pulse repetition rates. As illustrated in Figure 2, a positive correlation between pulse energy and height was observed.

Following the same methodology, the investigation was extended to width. The experiment was replicated with identical pulse energy variations and repetition rates. As depicted in Figure 3, a corresponding increase in width was observed with increasing pulse energy and repetition rate. The percentage error was calculated for each width measurement.

4.2. Forecasts and Regression Results

In the discussion section of this study, it is imperative to scrutinize the predictive performance of the ANN as reflected by the forecasted results detailed in Table 3 and in Figure 4. The table presents a comprehensive set of evaluation metrics for both the height and width of the laser-induced tracks, providing a nuanced view of the model's accuracy and effectiveness.

For the forecasted track height, the model exhibits excellent predictive accuracy as indicated by the low MSE of 0.232%. This low percentage highlights the model's strong ability to predict height with minimal deviation from the actual measurements. The RMSE at 0.482% further supports this, indicating that the model's predictions are consistently close to the true data points. The MAE of 0.312% and the MAPE of 0.066% both reinforce the model's high precision, with the MAPE, in particular, showing very small deviation in terms of percentage, which is crucial for ensuring the practical applicability of the predictions in real-world settings. The CVRMSE at 10.241% provides a normalized measure of the RMSE, illustrating a relatively low spread in the error relative to the magnitude of the data being predicted. The R^2 for height is 0.909, signifying that a substantial proportion of the variability in track height is effectively captured by the model.

In contrast, the forecasted results for track width show a slightly higher level of error across the metrics, though they still indicate strong predictive performance. The MSE for width is notably higher at 2.601%, suggesting more variability in the model's predictions for width compared to height. Similarly, the RMSE at 1.613% and the MAE at 0.923% are higher than those for height, implying that the predictions for width are less consistent. However, these values still demonstrate a high level of accuracy overall. The MAPE for width is slightly higher at 0.116%, but it remains low, affirming the model's utility in practical applications. The CVRMSE at 12.141% is higher than that for height, indicating a greater relative spread in the error for width predictions. The R^2 value for width, at 0.902, remains high, which confirms that the model successfully captures a large portion of the variability in track width. The regression line and error histogram for the height and width forecasted features

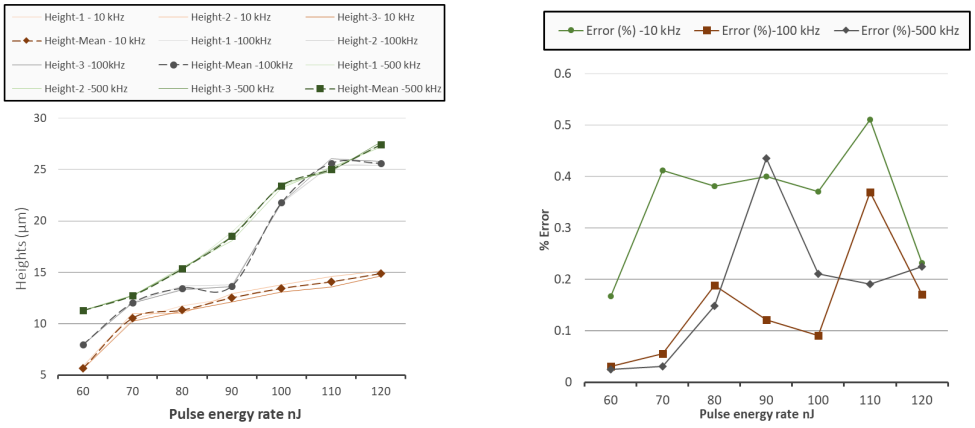

[!ht] (a) (b)

Figure 2: Pulse repetition rate and energy track height results: (a) Height; (b) Error percentage.

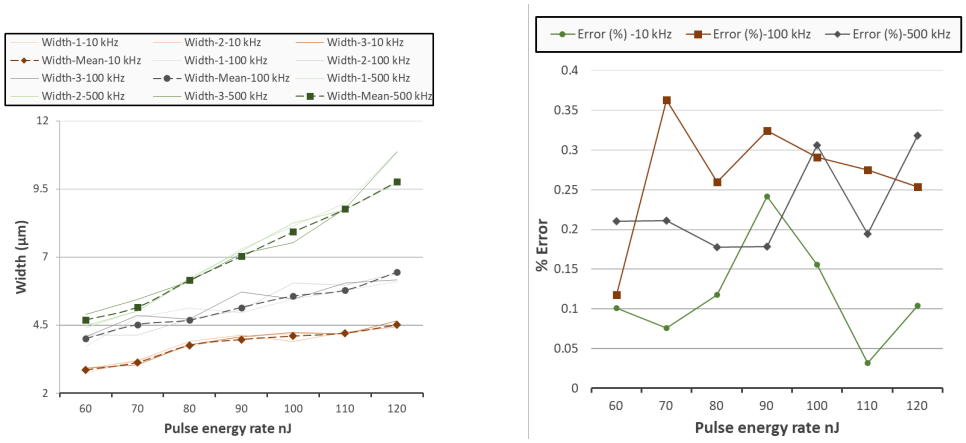

(a) (b)

Figure 3: Pulse repetition rate and energy track width results: (a) Width; (b) Error percentage.

are depicted in Figures 5 and 6, respectively.

The comparative analysis between the metrics for height and width forecasts suggests that while the model is slightly more accurate and consistent in predicting height, its performance in predicting width is commendably high. Both sets of metrics underscore the ANN model's robustness and its potential as a predictive tool in laser material processing. These results validate the model's capability to assist in optimizing processing parameters for femtosecond laser applications, particularly in settings where precision and repeatability are paramount.

[htbp]

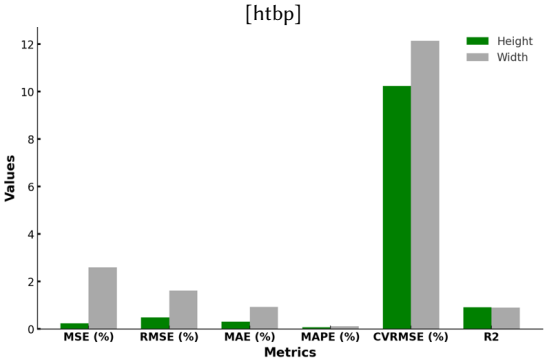

Figure 4: Assessment metrics depiction.

Table 3
Forecasted results

Forecasts	MSE (%)	RMSE (%)	MAE (%)	MAPE (%)	CVRMSE (%)	R^2
Height	0.232	0.482	0.312	0.066	10.241	0.909
Width	2.601	1.613	0.923	0.116	12.141	0.902

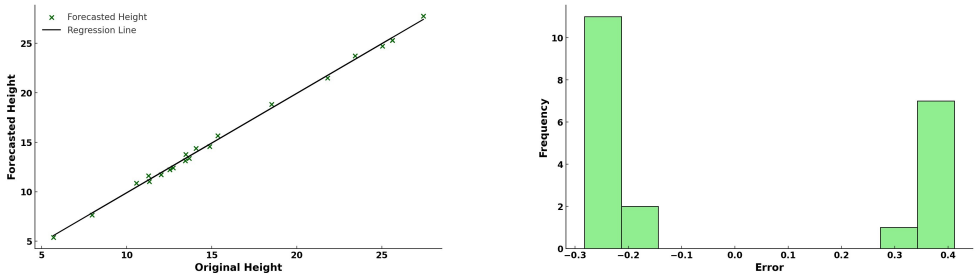

(a) (b)

Figure 5: Height forecasts: (a) Regression line; (b) Error histogram.

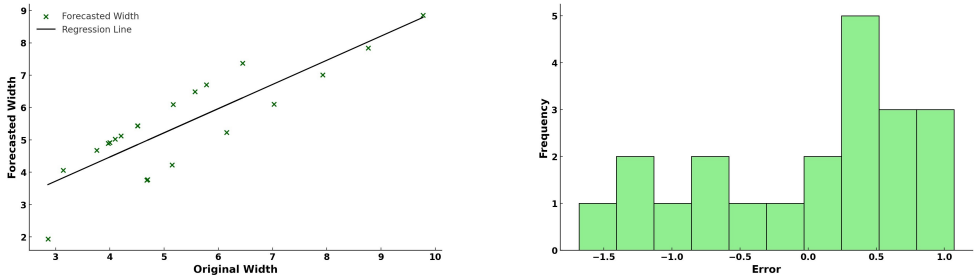

(a) (b)

Figure 6: Forecasts of width: (a) Regression line; (b) Error histogram.

5. Conclusions and Future Directions

This study successfully implemented an ANN to predict the dimensions of femtosecond laser-induced tracks in silver-containing zinc phosphate glass. The model demonstrated high accuracy, as evidenced by low MSE and RMSE values, particularly in predicting the height of laser-written tracks. The MAE and CVRMSE further validated the precision of the predictions. Significantly, the R^2 indicated that a substantial portion of the variance in both height and width of the tracks was captured by the ANN model. These results underscored the capability of advanced machine learning techniques to enhance the predictability and optimization of laser processing applications.

Future studies can carry out the preliminary investigation set by this work using more input variables in the model, such as material variability and ambient conditions, for deeper accuracy in prediction. Experimenting with various network architectures and deep-learning models, one could further shed more insights into the complex interaction within the laser processing domain. More interesting, practical, and real-time implementation of the developed ANN model can be achieved for the better results of the laser manufacturing process. Further, the developed models can be used to predict other families of glasses and other types of lasers. From another point of view, this work will contribute to the general scope of materials engineering in as much as it makes further development of much finer and more reliable laser fabrication methods possible.

References

[1] J. Zhang, Q. Zhao, D. Du, Y. Zhu, S. Zheng, D. Chen, J. Cui, High flexibility fbg inscribing by point-by-point method via femtosecond laser:

Technology, progress, and challenges, Materials Today Communications 39 (2024) 108760. URL: https://www.sciencedirect.com/science/article/pii/S2352492824007414. doi:https://doi.org/10.1016/j.mtcomm.2024.108760.

[2] G. Lo Sciuto, G. Capizzi, R. Shikler, C. Napoli, Organic solar cells defects classification by using a new feature extraction algorithm and an ebnn with an innovative pruning algorithm, International Journal of Intelligent Systems 36 (2021) 2443–2464.

[3] G. Lo Sciuto, G. Capizzi, S. Coco, R. Shikler, Geometric shape optimization of organic solar cells for efficiency enhancement by neural networks, in: Advances on Mechanics, Design Engineering and Manufacturing: Proceedings of the International Joint Conference on Mechanics, Design Engineering & Advanced Manufacturing (JCM 2016), 14-16 September, 2016, Catania, Italy, Springer, 2017, pp. 789–796.

[4] R. Giuliano, F. Mazzenga, A. Vizzarri, Integration of broadcaster and telco access networks for real time/live events, IEEE Transactions on Broadcasting 66 (2020) 667–675. doi:10.1109/TBC.2020.2965057.

[5] F. Fiani, S. Russo, C. Napoli, An advanced solution based on machine learning for remote emdr therapy, Technologies 11 (2023). doi:10.3390/technologies11060172.

[6] R. Giuliano, F. Mazzenga, E. Innocenti, A. Vizzarri, Integration of video and radio technologies for social distancing, IEEE Communications Magazine (2021) 30–35.

[7] I. E. Tibermacine, A. Tibermacine, W. Guettala, C. Napoli, S. Russo, Enhancing sentiment analysis on seed-iv dataset with vision transformers: A comparative study, in: ACM International Conference Proceeding Series, 2023, p. 238 – 246. doi:10.1145/3638985.3639024.

[8] E. Iacobelli, S. Russo, C. Napoli, A machine learning based real-time application for engagement detection, in: CEUR Workshop Proceedings, volume 3695, 2023, p. 75 – 84.

[9] R. Giuliano, E. Innocenti, F. Mazzenga, A. Vizzarri, L. Di Nunzio, P. Divakarachari, I. Habib, Transformer neural network for throughput improvement in non-terrestrial networks, MDPI networks (2023) 1–6. doi:10.1109/NMITCON58196.2023.10276347.

[10] S. Danto, F. Désévédavy, Y. Petit, J.-C. Desmoulin, A. Abou Khalil, C. Strutynski, M. Dussauze, F. Smektala, T. Cardinal, L. Canioni, Photowritable silver-containing phosphate glass ribbon fibers, Advanced Optical Materials 4 (2016) 162–168. URL: https://onlinelibrary.wiley.com/doi/abs/10.1002/adom.201500459. doi:https://doi.org/10.1002/adom.201500459.

[11] C. Cai, J. Wang, Femtosecond laser-fabricated photonic chips for optical communications: A review, Micromachines 13 (2022). URL: https://www.mdpi.com/2072-666X/13/4/630. doi:10.3390/mi13040630.

[12] L. Canioni, Y. Petit, T. Cardinal, Nanostructuring by Photochemistry: Laser-Induced Type A Modification, Springer International Publishing, Cham, 2023, pp. 691–723. URL: https://doi.org/10.1007/978-3-031-14752-4_19. doi:10.1007/978-3-031-14752-4_19.

[13] J. Harb, T. Guérineau, A. Morana, A. Meyer, G. Raffy, A. D. Guerzo, Y. Ouerdane, A. Boukenter, S. Girard, T. Cardinal, Y. Petit, L. Canioni, Femtosecond direct laser writing of silver clusters in phosphate glasses for x-ray spatially-resolved dosimetry, Chemosensors 10 (2022). URL: https://www.mdpi.com/2227-9040/10/3/110. doi:10.3390/chemosensors10030110.

[14] N. Marquestaut, Y. Petit, A. Royon, P. Mounaix, T. Cardinal, L. Canioni, Three-dimensional silver nanoparticle formation using femtosecond laser irradiation in phosphate glasses: Analogy with photography, Advanced Functional Materials 24 (2014) 5824–5832. URL: https://onlinelibrary.wiley.com/doi/abs/10.1002/adfm.201401103. doi:https://doi.org/10.1002/adfm.201401103.

[15] G. Shakhgildyan, A. Lipatiev, M. Vetchinnikov, V. Popova, S. Lotarev, N. Golubev, E. Ignat'eva, M. Presniakov, V. Sigaev, One-step micro-modification of optical properties in silver-doped zinc phosphate glasses by femtosecond direct laser writing, Journal of Non-Crystalline Solids 481 (2018) 634–642. URL: https://www.sciencedirect.com/science/article/pii/S002230931730666X. doi:https://doi.org/10.1016/j.jnoncrysol.2017.12.011.

[16] G. Shakhgildyan, A. Lipatiev, S. Fedotov, M. Vetchinnikov, S. Lotarev, V. Sigaev, Microstructure and optical properties of tracks with precipitated silver nanoparticles and clusters inscribed by the laser irradiation in phosphate glass, Ceramics International 47 (2021) 14320–14329. URL: https://www.sciencedirect.com/science/article/pii/S027288422100345X. doi:https://doi.org/10.1016/j.ceramint.2021.02.012.

[17] E. Iacobelli, V. Ponzi, S. Russo, C. Napoli, Eye-tracking system with low-end hardware: Development and evaluation, Information (Switzerland) 14 (2023). doi:10.3390/info14120644.

[18] F. Alassani, G. Galleani, G. Raffy, A. Del Guerzo, A. Royon, K. Bourhis, A. S. S. de Camargo, V. Jubera, L. Canioni, T. Cardinal, Y. Petit, (invited)direct laser writing of visible and near infrared 3d lumi-

nescence patterns in glass, Optical Materials: X 16 (2022) 100205. URL: https://www.sciencedirect.com/science/article/pii/S2590147822000699. doi:https://doi.org/10.1016/j.omx.2022.100205.

[19] F. Bonanno, G. Capizzi, S. Coco, C. Napoli, A. Laudani, G. L. Sciuto, Optimal thicknesses determination in a multilayer structure to improve the spp efficiency for photovoltaic devices by an hybrid fem - cascade neural network based approach, 2014, pp. 355 – 362. doi:10.1109/SPEEDAM.2014.6872103.

[20] J. Lv, G. Zhang, J. Wang, K. Wang, G. Cheng, Cladding waveguide fabrication by femtosecond laser in yb-doped phosphate glasses, Optics amd Laser Technology 169 (2024) 110167. URL: https://www.sciencedirect.com/science/article/pii/S0030399223010605. doi:https://doi.org/10.1016/j.optlastec.2023.110167.

[21] K. Tsimvrakidis, I. Konidakis, E. Stratakis, Laser-induced erasable and re-writable waveguides within silver phosphate glasses, Materials 15 (2022). URL: https://www.mdpi.com/1996-1944/15/9/2983.

[22] T. Guérineau, A. Fargues, J. Lapointe, R. Vallée, Y. Messaddeq, L. Canioni, Y. Petit, T. Cardinal, Laser direct writing of silver clusters-based subwavelength periodic structures embedded in mid-infrared gallo-germanate glass, Advanced Photonics Research 3 (2022) 2200032. URL: https://onlinelibrary.wiley.com/doi/abs/10.1002/adpr.202200032. doi:https://doi.org/10.1002/adpr.202200032.

[23] J.-C. Desmoulin, Y. Petit, L. Canioni, M. Dussauze, M. Lahaye, H. M. Gonzalez, E. Brasselet, T. Cardinal, Femtosecond laser structuring of silver-containing glass: Silver redistribution, selective etching, and surface topology engineering, Journal of Applied Physics 118 (2015).

[24] M. Bukharin, D. Khudyakov, S. Vartapetov, Heat accumulation regime of femtosecond laser writing in fused silica and nd: phosphate glass, Applied Physics A 119 (2015) 397–403.

[25] T. Guérineau, L. Loi, Y. Petit, S. Danto, A. Fargues, L. Canioni, T. Cardinal, Structural influence on the femtosecond laser ability to create fluorescent patterns in silver-containing sodium-gallium phosphate glasses, Opt. Mater. Express 8 (2018) 3748–3760. URL: https://opg.optica.org/ome/abstract.cfm?URI=ome-8-12-3748. doi:10.1364/OME.8.003748.

[26] T. Guérineau, F. Cova, Y. Petit, A. Abou Khalil, A. Fargues, M. Dussauze, S. Danto, A. Vedda, L. Canioni, T. Cardinal, Silver centers luminescence in phosphate glasses subjected to x-rays or combined x-rays and femtosecond laser exposure, International Journal of Applied Glass Science 11 (2020) 15–26. URL: https://ceramics.onlinelibrary.wiley.com/doi/abs/10.1111/ijag.13957. doi:https://doi.org/10.1111/ijag.13957.

[27] G. Shakhgildyan, A. Lipatiev, M. Vetchinnikov, S. Fedotov, S. Lotarev, V. Sigaev, Data on the femtosecond laser-induced formation of tracks in silver-containing zinc phosphate glass, Data in Brief 34 (2021) 106698. URL: https://www.sciencedirect.com/science/article/pii/S2352340920315778. doi:https://doi.org/10.1016/j.dib.2020.106698.

[28] A. Lipat'ev, M. Vetchinnikov, G. Y. Shakhgil'dyan, S. Lotarev, A. Vasetskii, V. Sigaev, Controlling the optical characteristics of laser-induced microstructures in zinc phosphate glass containing silver, Glass and Ceramics 74 (2018) 385–388.

[29] C. A. Schneider, W. S. Rasband, K. W. Eliceiri, Nih image to imagej: 25 years of image analysis, Nature methods 9 (2012) 671–675.

[30] L. A. Al-Haddad, N. M. Mahdi, Efficient multidisciplinary modeling of aircraft undercarriage landing gear using data-driven naïve bayes and finite element analysis, Multiscale and Multidisciplinary Modeling, Experiments and Design (2024) 1–13.

[31] C. Napoli, F. Bonanno, G. Capizzi, An hybrid neuro-wavelet approach for long-term prediction of solar wind, in: Proceedings of the International Astronomical Union, volume 6, 2010, p. 153 – 155. doi:10.1017/S174392131100679X.

[32] L. A. Al-Haddad, A. A. Jaber, M. N. Hamzah, M. A. Fayad, Vibration-current data fusion and gradient boosting classifier for enhanced stator fault diagnosis in three-phase permanent magnet synchronous motors, Electrical Engineering (2023) 1–16.

[33] F. Bonanno, G. Capizzi, C. Napoli, Some remarks on the application of rnn and prnn for the charge-discharge simulation of advanced lithium-ions battery energy storage, in: SPEEDAM 2012 - 21st International Symposium on Power Electronics, Electrical Drives, Automation and Motion, 2012, p. 941 – 945. doi:10.1109/SPEEDAM.2012.6264500.

[34] L. A. Al-Haddad, S. S. Shijer, A. A. Jaber, S. T. Al-Ani, A. A. Al-Zubaidi, E. T. Abd, Application of adaboost for stator fault diagnosis in three-phase permanent magnet synchronous motors based on vibration–current data fusion analysis, Electrical Engineering (2024) 1–16.

[35] F. Bonanno, G. Capizzi, G. L. Sciuto, C. Napoli, G. Pappalardo, E. Tramontana, A novel cloud-distributed toolbox for optimal energy dispatch management from renewables in igss by using wrnn predictors and gpu parallel solutions, in: 2014 International Symposium on Power Electronics, Electrical Drives, Automation and Motion, SPEEDAM 2014, 2014, p. 1077 – 1084. doi:10.1109/SPEEDAM.2014.6872127.

[36] L. A. Al-Haddad, W. H. Alawee, A. Basem, Advancing task recognition towards artificial limbs control with relieff-based deep neural network extreme learning, Computers in Biology and Medicine 169 (2024) 107894. URL: https://www.sciencedirect.com/science/article/pii/S0010482523013598. doi:https://doi.org/10.1016/j.compbiomed.2023.107894.

[37] L. A. Al-Haddad, A. A. Jaber, Applications of machine learning techniques for fault diagnosis of uavs., SYSTEM (2022) 19–25.

[38] L. A. Al-Haddad, A. A. Jaber, Improved uav blade unbalance prediction based on machine learning and relieff supreme feature ranking method, Journal of the Brazilian Society of Mechanical Sciences and Engineering 45 (2023) 463.

[39] M. Y. Fattah, L. A. Al-Haddad, M. Ayasrah, A. A. Jaber, S. A. Al-Haddad, Coupled finite element and artificial neural network analysis of interfering strip footings in saturated cohesive soils, Transportation Infrastructure Geotechnology (2024) 1–18.

[40] G. Capizzi, G. L. Sciuto, C. Napoli, M. Woźniak, G. Susi, A spiking neural network-based long-term prediction system for biogas production, Neural Networks 129 (2020) 271 – 279. doi:10.1016/j.neunet.2020.06.001.

[41] L. A. Al-Haddad, Y. M. Al-Muslim, A. S. Hammood, A. A. Al-Zubaidi, A. M. Khalil, Y. Ibraheem, H. J. Imran, M. Y. Fattah, M. F. Alawami, A. M. Abdul-Ghani, Enhancing building sustainability through aerodynamic shading devices: an integrated design methodology using finite element analysis and optimized neural networks, Asian Journal of Civil Engineering (2024) 1–14.

[42] L. A. Al-Haddad, A. A. Jaber, An intelligent quadcopter unbalance classification method based on stochastic gradient descent logistic regression, in: 2022 3rd Information Technology To Enhance e-learning and Other Application (IT-ELA), 2022, pp. 152–156. doi:10.1109/IT-ELA57378.2022.10107922.

[43] G. De Magistris, S. Russo, P. Roma, J. T. Starczewski, C. Napoli, An explainable fake news detector based on named entity recognition and stance classification applied to covid-19, Information (Switzerland) 13 (2022). doi:10.3390/info13030137.

[44] L. A. Al-Haddad, A. A. Jaber, An intelligent fault diagnosis approach for multirotor uavs based on deep neural network of multi-resolution transform features, Drones 7 (2023). URL: https://www.mdpi.com/2504-446X/7/2/82. doi:10.3390/drones7020082.

[45] L. A. Al-Haddad, A. A. Jaber, S. A. Al-Haddad, Y. M. Al-Muslim, Fault diagnosis of actuator damage in uavs using embedded recorded data and stacked machine learning models, The Journal of Supercomputing 80 (2024) 3005–3024.

[46] F. Bonanno, G. Capizzi, A. Gagliano, C. Napoli, Optimal management of various renewable energy sources by a new forecasting method, in: SPEEDAM 2012 - 21st International Symposium on Power Electronics, Electrical Drives, Automation and Motion, 2012, p. 934 – 940. doi:10.1109/SPEEDAM.2012.6264603.

[47] A. A. F. Ogaili, M. N. Hamzah, A. A. Jaber, Enhanced fault detection of wind turbine using extreme gradient boosting technique based on nonstationary vibration analysis, Journal of Failure Analysis and Prevention 24 (2024) 877–895.

[48] A. A. F. Ogaili, A. A. Jaber, M. N. Hamzah, A methodological approach for detecting multiple faults in wind turbine blades based on vibration signals and machine learning, Curved and Layered Structures 10 (2023) 20220214.

[49] G. C. Cardarilli, L. Di Nunzio, R. Fazzolari, D. Giardino, M. Re, A. Ricci, S. Spanò, An fpga-based multi-agent reinforcement learning timing synchronizer, Computers and Electrical Engineering 99 (2022) 107749. URL: https://www.sciencedirect.com/science/article/pii/S0045790622000581. doi:https://doi.org/10.1016/j.compeleceng.2022.107749.

[50] F. Bonanno, G. Capizzi, G. Lo Sciuto, A neuro wavelet-based approach for short-term load forecasting in integrated generation systems, in: 2013 International Conference on Clean Electrical Power (ICCEP), IEEE, 2013, pp. 772–776.

[51] G. C. Cardarilli, L. Di Nunzio, R. Fazzolari, D. Giardino, M. Matta, M. Patetta, M. Re, S. Spanò, Approximated computing for low power neural networks, Telkomnika (Telecommunication Computing Electronics and Control) 17 (2019) 1236–1241.

[52] W. H. Alawee, L. A. Al-Haddad, A. Basem, D. J. Jasim, H. S. Majdi, A. J. Sultan, Forecasting sustainable water production in convex tubular solar stills using gradient boosting analysis, Desalination and Water Treatment 318 (2024) 100344. URL: https://www.sciencedirect.com/science/article/pii/S1944398624003771. doi:https://doi.org/10.1016/j.dwt.2024.100344.

[53] S. A. Mohammed, L. A. Al-Haddad, W. H. Alawee, H. A. Dhahad, A. A. Jaber, S. A. Al-Haddad, Forecasting the productivity of a solar distiller enhanced with an inclined absorber plate using stochastic gradient descent in artificial neural networks, Multiscale and Multidisciplinary Modeling, Experiments and Design (2023) 1–11.